PCCP

RSC Publishing

PAPER

View Article Online
View Journal | View Issue

Cite this: *Phys. Chem. Chem. Phys.*, 2013, **15**, 18410

Coinage metal exciplexes with helium atoms: a theoretical study of M*(^{2}L)He$_n$ (M = Cu, Ag, Au; L = P,D)

Fausto Cargnoni,[a] Alessandro Ponti[a] and Massimo Mella*[b]

Received 19th January 2013,
Accepted 6th September 2013

DOI: 10.1039/c3cp50250c

www.rsc.org/pccp

The structure and energetics of exciplexes M*(^{2}L)He$_n$ (M = Cu, Ag and Au; L = P and D) in their vibrational ground state are studied by employing diffusion Monte Carlo (DMC). Interaction potentials between the excited coinage metals and He atoms are built using the Diatomics-in-Molecule (DIM) approach and *ab initio* potential curves for the M(^{2}L)–He dimers. Extending our previous work [Cargnoni *et al., J. Phys. Chem. A*, 2011, **115**, 7141], we computed the dimer potential for Au in the ^{2}P and ^{2}D states, as well for Cu and Ag in the ^{2}D state, employing basis set superposition error-corrected Configuration Interaction calculations. We found that the $^2\Pi$ potential correlating with the ^{2}P state of Au is substantially less binding than for Ag and Cu, a trend well supported by the M$^+$ ionic radiuses. Conversely, the interaction potentials between a $(n-1)d^9ns^2$ ^{2}D metal and He present a very weak dependency on M itself or the projection of the angular momentum along the dimer axis. This is due to the screening exerted by the ns^2 electrons on the hole in the $(n-1)$d shell. Including the spin–orbit coupling perturbatively in the DIM energy matrix has a major effect on the lowest potential energy surface of the ^{2}P manifold, the one for Cu allowing the formation of a ''belt'' of five He atoms while the one for Au being completely repulsive. Conversely, spin–orbit coupling has only a weak effect on the ^{2}D manifold due to the nearly degenerate nature of the diatomic potentials. Structural and energetic results from DMC have been used to support experimental indications for the formation of metastable exciplexes or the opening of non-radiative depopulation channels in bulk and cold gaseous He.

1 Introduction

Rationalising the post-excitation dynamics of a chromophore experiencing a condensed phase environment requires, often, invoking the presence of aggregates formed between the excited moiety and a few solvent molecules initially lying close to it. Of interest to us in this context, are the many photo-excitation experiments carried out in bulk ^{4}He,[1–9] using ^{4}He droplets to extract subtle features of the light absorbing species exploiting the weakly interacting nature of such nano-cryostats,[10–18] or in cold helium gas.[19–23]

Despite the weakly interacting nature of helium, electronic photo-excitation of atomic dopants embedded into its bulk or on a droplet surface tends, nevertheless, to be markedly affected by the surrounding matrix. Thus, absorption spectra may be strongly shifted and substantially broadened in the case of embedded dopants,[1,2,12,13] or may present a long tail in the blue of the free transition frequency for floating species.[10,11,14–16,24] As for emission spectroscopy, lines often disappear or are strongly redshifted, suggesting the formation of complexes between the excited chromophore and the He atoms, usually dubbed ''exciplexes''.[1,3,4,6,8,9,14–17,19] It is suggested that this could happen also in cold gases,[19–23] a process perhaps mediated by collisional energy dissipation.

Investigating the processes leading to the formation of exciplexes and their fate from the theoretical point of view necessitates, as a basic ingredient, accurate interaction potential surfaces between the excited moiety and one or more He atoms. As those potentials require the use of *ab initio* methods and basis sets specifically apt to dealing with excited states, the computational effort involved in obtaining the latter tends to be substantially higher than for the ground state potentials. This is true also for species that already require a multi-state approach to investigate their ground state interactions due, for instance, to a non-zero electronic orbital momentum.[25] As a consequence of such higher cost, only a few theoretical studies have, so far, been devoted to investigate the structure, energetics and dynamics of exciplexes[26–33] providing the needed support for the interpretation of experimental results. It is also worth mentioning the fact that there are cases (see *e.g.* the ^{2}P ← ^{2}S

[a] *Istituto di Scienze e Tecnologie Molecolari (ISTM), Consiglio Nazionale delle Ricerche, via Golgi 19, 20133 Milano, Italy. E-mail: fausto.cargnoni@istm.cnr.it, alessandro.ponti@istm.cnr.it*

[b] *Dipartimento di Scienza ed Alta Tecnologia, Università degli Studi dell'Insubria, via Lucini 3, 22100 Como, Italy. E-mail: massimo.mella@uninsubria.it*

case of Cu[34]) for which the task of computing excited state surfaces is made even more demanding as the ones needed for the state accessible *via* photo-excitation do not correlate with the first excited manifold (*i.e.* the ^{2}D one for Cu), but rather with higher roots of the secular Configuration Interaction (CI) system.

An additional hurdle in obtaining key pieces of information on exciplexes is represented by the marked anharmonic nature of their vibrational modes. This prevents one from approaching the investigation with the customary geometry optimisation followed by a harmonic (or even perturbatively anharmonic) analysis using the most appropriate *ab initio* level, and it imposes instead the use of quantum simulation methods. The latter, in turn, introduce the necessity for an efficient calculation of the interaction energy due to the extensive configurational sampling, placing out of reach its ''on the fly'' computation with *ab initio* methods. Consequently, one is forced to rely on approximations such as the Diatomics-in-Molecules approach,[35] a perturbation method capable of building a multi-state representation of the many-body interaction surface starting from atomic and diatomic data. As it also allows us to easily introduce spin–orbit coupling, albeit at the cost of doubling the matrix sizes, it is chosen by us to generate the energy surfaces needed to study the properties of exciplexes.

The goal of this work is to investigate the structural and energetic properties of M*(^{2}L)He$_n$ exciplexes (M = Cu, Ag and Au, and L = P,D), a task that we undertook with a two-pronged approach (*vide infra*). The reasons for applying ourselves to this task are related to the fact that these species have been invoked to interpret several experimental results[1,8,9,19] such as the disappearance of the D2 emission for all the metals in bulk He,[1,8,9] the non-radiative population of the $^2P_{1/2}$ state of Ag in bulk He[1,36] and cold He gas,[19] the long and temperature-dependent lifetime of the D1 and Ag($^2P_{3/2}$)He$_2$ fluorescence lines, and the appearance of the $^2D_{5/2,3/2} \rightarrow {}^2S$ emission by Cu in bulk He[8,9] following its excitation into the ^{2}P manifold. Despite these experimental indications, only the existence and properties of Ag($^2P_{3/2}$)He and Ag($^2P_{3/2}$)He$_2$ have so far received sufficient support from theoretical studies.[1,27,33,34] Even these cases, however, warrant a re-investigation owing to the recent observation[34] of a likely overbinding nature of the potentials in ref. 27. It however appears to be unlikely that this would lead to different conclusions on their stability. Differently, this may happen when it comes to the larger aggregates previously indicated for $^2P_{1/2}$ Ag,[33] the potential for the $^2\Pi_{1/2}$ state of Ag–He appearing substantially less binding when computed with higher level *ab initio* approaches[34] than before.[27]

As hinted in the preceding discussion, we first computed all the needed diatomic interaction potentials (*i.e.* the ones between ^{2}P Au and He, as well as between He and the three metals in the ^{2}D state), and subsequently simulated the vibrational ground state properties for the M*(^{2}L)He$_n$ aggregates with diffusion Monte Carlo (DMC). The rationale behind our choice for using a ground state approach such as DMC is twofold. On one hand, the potential energy surface for the interesting coinage metal states (*i.e.* the ones that form exciplexes) is either almost or completely barrierless with respect to a He atom approaching the metal from long distances (*vide infra* Sections 4.1 and 4.2). Thus, there is nothing preventing He atoms to come closer to the de-screened metal nucleus after excitation. On the other hand, the diffusion of He atoms in cluster and bulk helium is quite fast (it is estimated that it takes roughly 40 ps to diffuse an average of 20 Å[37]) even at a cluster temperature of 0.4 K. These facts, together with the fast energy dissipation afforded by the surrounding helium atoms,[37] make it highly probable that the first shell solvent He atoms around the metal can be ''drawn in'' by the stronger interaction generated by the asymmetric P electron density induced by the excitation well before the metal atom is allowed to relax to its ground electronic state (with lifetime of the order of nanoseconds). Thus, provided one is not interested in the details of the dynamics ensuing after the photon adsorption, DMC appears to be a valid method to study the structural details of the complex formed and sheds some light on their fate.

The details of the *ab initio* calculations for the interaction energies and their results are described in Section 2. Section 3 provides details on the DMC approach and the DIM method used to model the structure and energetics of the studied exciplexes, the results and relevance of our investigation being described in Section 4. Finally, Section 5 provides our conclusions and indications for future work in this arena.

2 *Ab initio* potential energy curves

In a recent investigation,[34] we performed *ab initio* Configuration Interaction (CI) calculations on the Cu–He and Ag–He dimers to determine the excited state potentials (PES) that correlate asymptotically with the lowest lying ^{2}P atomic doublets of the metal atom. In the present study we computed these PES also for the Au–He system; for each M–He complex (M = Cu, Ag, Au) we also investigated the five lowest lying excited states correlating asymptotically with the ^{2}D atomic doublets.

The ^{2}P excited states of the metal atom arise from the excitation of an electron from the outermost s orbital to the empty p shell, and hence the outer electronic configuration is $(n-1)d^{10}np^1$ (n = 4, 5, 6 for Cu, Ag and Au, respectively). In the ^{2}D states one electron is promoted from the filled d shell of the metal atom to its half-filled s shell, and the corresponding electronic configuration is $(n-1)d^9ns^2$. Overall, the states considered here are the $^2\Sigma^+$, $^2\Pi_{1/2}$ and $^2\Pi_{3/2}$ states of M–He dimers which correlate asymptotically with the ^{2}P doublets of Cu, Ag and Au, and the $^2\Sigma^+$, $^2\Pi_{1/2}$, $^2\Pi_{3/2}$, $^2\Delta_{3/2}$ and $^2\Delta_{5/2}$ states which correlate asymptotically with the atomic ^{2}D doublets. We anticipate here that these excited states of the M–He dimers (M = Cu, Ag, Au) retain a strong atomic character in all computations, and hence the helium atom behaves essentially as a probe to explore the electronic structure of an excited copper, silver or gold atom.

The entire set of interaction potentials has been determined following closely the computational procedure already adopted for Ag–He, and extensively described in ref. 34. We report below a brief summary of our CI approach, and we address the interested reader to our previous investigation for more

extensive details. In addition, the lowest lying state of each symmetry has been determined also at the UCCSD(T) level of theory.

In all computations the inner electrons of Cu, Ag and Au are described with the relativistic small-core pseudo-potentials (PP) proposed by Figgen *et al.*[38] The M–He (M = Cu, Ag, Au) dimers are then treated as 21 electron systems: two $1s^2$ electrons on helium, and the 19 outermost electrons on the metal atoms: $3s^23p^63d^{10}4s^1$ for Cu, $4s^24p^64d^{10}5s^1$ for Ag and $5s^25p^65d^{10}6s^1$ for Au. The spin–orbit coupling has been neglected at this stage, and it is included *a posteriori*, according to the scheme adopted in ref. 27 and 39 for the ^{2}P states, and that is extended in this work to the ^{2}D states. Configuration Interaction computations have been performed with the GAMESS-US code,[40] while UCCSD(T) calculations were performed with the MOLPRO code.[41–43] The interaction energy data have been corrected using the standard counterpoise technique proposed by Boys and Bernardi.[44] In the discussion below, the asymptotes of all interaction potentials have been set to be zero. The concepts of the "well depth", "attractive" and "repulsive" region of the PES should therefore be interpreted according to this choice.

The CI potentials have been determined with a two step strategy, including electron correlation coming from the 13 outermost electrons of M–He complexes. First, we assigned to M–He complexes a *small* basis set, we performed CI computations including up to triple excitations (CISDT), and we defined for each electronic state an analytical expression for the contribution of triple excitations. Second, we selected a basis set with a much larger flexibility, from now on referred to as *large*, and we computed the interaction potentials including single and double excitations (CISD). The final CI potentials have been defined summing up interaction energies obtained with the *large* basis set and the contribution of triple excitations as determined with the *small* basis.

The *small* basis set contains just 37 Gaussian functions, and is obtained assigning the cc-pVDZ[45] basis set (with the exclusion of the single set of f functions) to the metal atoms, the aug-cc-pVDZ[46] to He, and placing a 1s1p set of bond functions at midway between the M and He nuclei. As discussed extensively in our previous investigation,[34] the *small* basis set proved to be flexible enough to recover the main features of the PES under investigation. The *large* basis set consists of 173 Gaussian functions, and contains the aug-cc-pVTZ[45] set for the metal atom, the d-aug-cc-pVTZ[46] set for He, and a 3s3p2d[47] set of bond functions placed at midway between the M and He nuclei.

Details of CI computations are as follows: the CISD to CISDT difference, determined with the *small* basis set, has been computed at 28 internuclear distances in the range from 1.6 to 10.0 Å in the Cu–He complex, at 32 distances in the range from 2.0 to 10.0 Å in Ag–He, and 23 distances in the same range in the Au–He dimer. CISD computations with the *large* basis set have been performed at 32 internuclear distances from 1.6 to 10.0 Å in Cu–He, 33 internuclear distances from 2.075 to 10.0 Å in Ag–He, and 37 internuclear distances from 2.0 to 10.0 Å in Au–He. The internuclear distances have been selected to sample finely the regions where the interaction potentials undergo sudden changes. UCCSD(T) computations have been performed with the *large* basis set at the same internuclear distances considered in CISD calculations. In all computations we adopted a ROHF reference wavefunction. The electronic excited states available at the UCCSD(T) level of theory are the $^2\Pi_{1/2}$ and $^2\Pi_{3/2}$ states that correlate asymptotically with the ^{2}P doublets in Ag–He, and $^2\Delta_{3/2}$ and $^2\Delta_{5/2}$ that correlate with the ^{2}D atomic state. In the case of Cu–He and Au–He, we determined the interaction potentials of $^2\Pi_{1/2}$, $^2\Pi_{3/2}$, $^2\Delta_{3/2}$ and $^2\Delta_{5/2}$ states which correlate asymptotically with the atomic ^{2}D doublets. The $^2\Sigma^+$ ground state is clearly available in all systems. Both CI and UCCSD(T) potentials have been fitted using quintic splines set over the entire set of data available, forcing a

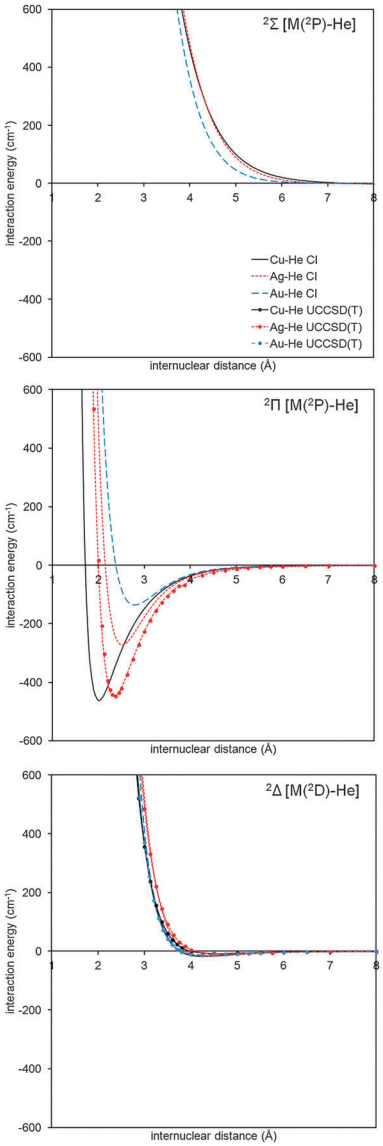

Fig. 1 Potential energy surfaces computed for different electronic states of M–He complexes using the *large* basis set. The CI $^2\Sigma^+$and $^2\Pi$ states of Cu–He and Ag–He dimers which correlate asymptotically with the ^{2}P atomic doublets are taken from ref. 34. Note that for each metal atom a single excited state correlating with the ^{2}D atomic doublet is reported (the $^2\Delta$ state), because these curves are indistinguishable in the range of the plot.

Table 1 Relevant properties of the excited state PES of M–He dimers (M = Cu, Ag, Au) without including the spin–orbit coupling and with the asymptotic interaction (asymptotic state ^{2}L) energy set to zero

M	Method	^{2}L	States	r_{min} [a]	E_{min} [b]	σ [c]
Cu	CCSDT	^{2}S	GS[d]	4.59	−6.2	4.04
Cu	CI	^{2}P	$^2\Sigma^+$ [e]	8.68	−2.7	7.50
Cu	CI	^{2}P	$^2\Pi_{1/2}$, $^2\Pi_{3/2}$ [e]	2.03	−462.2	1.72
Cu	CI	^{2}D	$^2\Sigma^+$	4.34	−14.9	3.85
Cu	CI	^{2}D	$^2\Pi_{1/2}$, $^2\Pi_{3/2}$	4.32	−16.2	3.81
Cu	UCCSD(T)	^{2}D	$^2\Pi_{1/2}$, $^2\Pi_{3/2}$	4.68	−8.1	4.03
Cu	CI	^{2}D	$^2\Delta_{3/2}$, $^2\Delta_{5/2}$	4.26	−17.6	3.76
Cu	UCCSD(T)	^{2}D	$^2\Delta_{3/2}$, $^2\Delta_{5/2}$	4.66	−8.2	4.00
Ag	CCSDT	^{2}S	GS[d]	4.60	−7.4	4.04
Ag	CI	^{2}P	$^2\Sigma^+$ [e]	7.89	−1.1	7.01
Ag	CI	^{2}P	$^2\Pi_{1/2}$, $^2\Pi_{3/2}$ [e]	2.52	−272.7	2.15
Ag	UCCSD(T)	^{2}P	$^2\Pi_{1/2}$, $^2\Pi_{3/2}$	2.36	−447.5	2.00
Ag	CI	^{2}D	$^2\Sigma^+$	4.50	−15.6	3.98
Ag	CI	^{2}D	$^2\Pi_{1/2}$, $^2\Pi_{3/2}$	4.46	−15.3	3.95
Ag	CI	^{2}D	$^2\Delta_{3/2}$, $^2\Delta_{5/2}$	4.39	−17.1	3.89
Ag	UCCSD(T)	^{2}D	$^2\Delta_{3/2}$, $^2\Delta_{5/2}$	4.63	−8.8	4.04
Au	CCSDT	^{2}S	GS[d]	4.09	−15.3	3.60
Au	CI	^{2}P	$^2\Sigma^+$ [f]			
Au	CI	^{2}P	$^2\Pi_{1/2}$, $^2\Pi_{3/2}$ [e]	2.80	−136.6	2.38
Au	CI	^{2}D	$^2\Sigma^+$	4.32	−11.6	3.83
Au	CI	^{2}D	$^2\Pi_{1/2}$, $^2\Pi_{3/2}$	4.33	−11.3	3.86
Au	UCCSD(T)	^{2}D	$^2\Pi_{1/2}$, $^2\Pi_{3/2}$	4.33	−13.1	3.81
Au	CI	^{2}D	$^2\Delta_{3/2}$, $^2\Delta_{5/2}$	4.30	−11.8	3.83
Au	UCCSD(T)	^{2}D	$^2\Delta_{3/2}$, $^2\Delta_{5/2}$	4.19	−13.5	3.79

[a] Internuclear M–He distance (Å) at the minimum interaction energy. [b] Minimum interaction energy (cm^{-1}). [c] Internuclear distance where the PES becomes repulsive (Å). [d] Data taken from ref. 52. [e] Data taken from ref. 34. [f] This potential is repulsive along the entire range of internuclear distances considered.

smooth joint at 10.0 Å with a long-range term with expression $-C_6/r^6$. The final potentials are reported in Fig. 1, and their relevant properties are collected in Table 1.

To assess the reliability of our CI scheme, we compared the triple excitation corrected ground state PES with CCSD(T) results obtained with the *large* basis set. At the distance of the minimum interaction energy (as determined by CCSD(T) computations) the CI potentials recover about 80% of the correlation energy contribution in Cu–He and Au–He, and 90% in Ag–He from the CCSDT calculations. The role of triple excitations is quite small (about 3% in Cu–He and Au–He, 4% in Ag–He), and slightly improves the accuracy of CI results. This outcome is consistent with data for the excited states: triple excitations give a small contribution to the interaction energy in the entire range of distances considered, and become relevant only at very short internuclear separations. This suggests that that the interaction between an excited M atom (M = Cu, Ag, Au) in the ^{2}P and ^{2}D states and helium is well described by single and double excited configurations.

Quite interestingly, for each metal atom the CI potentials of the excited states asymptotically correlating with the ^{2}D atomic configuration are very similar to one another, which means that to change the hole of the d^9 shell has a negligible effect on the interaction between helium and the metal, as already observed for Sc–He.[48] Furthermore, these PES do not change significantly even by switching the metal atom, and in the range shown in Fig. 1 they are hardly distinguishable from one another. As for excited states correlating with M(^{2}P), the $^2\Sigma^+$ curves of copper and silver are very similar, while the potential is significantly softer (*i.e.* less repulsive) in the case of gold. A strong dependence of the potentials on the M atom is observed only in the case of $^2\Pi$ states asymptotically correlating with the atomic ^{2}P states. Cu–He exhibits the largest attractive well, and its repulsive wall is located at shorter distances as compared to Ag–He and Au–He. Ag–He presents intermediate properties, while Au–He has the shallowest attractive well and the repulsive wall located at largest distances. Interestingly, this trend is consistent with the ionic radii of the M^+ cations (Cu^+ 96 pm, Ag^+ 126 pm, Au^+ 137 pm),[49] which suggest that these interactions are dominated by the induction interaction of helium with the positive core of the metals.

UCCSD(T) computations on available excited states present relevant differences with CI ones. In the case of excitations correlating with the ^{2}D atomic states, UCCSD(T) data agree with the observations reported for CI potentials. First, the inner polarization of the d^9 shell has no relevant effect on the potential. Second, PES corresponding to different metal atoms are very close to one another. The gross features of CI and UCCSD(T) potentials are quite similar, and the CI to UCCSD(T) interaction energy difference remains quite small along the entire range of internuclear distances considered. However, in the case of Cu–He and Ag–He UCCSD(T) data exhibit a smaller well depth with respect to CI ones, and the distance of the minimum interaction energy is significantly shifted at larger values, while in Au–He the opposite trend is found.

In the case of the Ag–He complex, UCCSD(T) data are available also for the degenerate $^2\Pi$ states correlating with the ^{2}P atomic doublet, and our results agree quite well to available literature data.[50,51] The well depth of the UCCSD(T) interaction potential is much deeper than the CI one, and shifted at shorter internuclear separations. The repulsive wall as obtained by UCCSD(T) data is located at distances about 0.15 Å smaller than what found with the CI approach. The change in the parameters of the $^2\Pi$ state for Ag in its ^{2}P state appears to be large and difficult to justify based only on the different methods used. This can be appreciated from the comparison between dimer states correlating with the ^{2}S and ^{2}D cases, and from the fact that even at long distances the two curves differ despite the very similar structure for the wave functions. As such, we believe that these differences deserve further investigation, which is currently underway in our laboratories. Here, we briefly mention that a comparison between UCCSD and UCCSD(T) results highlighted a marked effect due to the perturbative triple corrections, which might introduce some contamination from different states.

3 Diffusion Monte Carlo method and Diatomics-in-Molecule potentials

3.1 Diffusion Monte Carlo (DMC)

The deeply fluxional nature of He aggregates, even in the presence of strongly binding dopants, limits the usefulness of methods based on the harmonic approximation for the potential or on atomic Gaussian functions to build an approximate wave

function. Density Functional Theory based approaches,[53] despite representing an useful tool for very large He droplets, show a few shortcomings when describing small and granular systems as the ones we intend to investigate in this work. Thus, we opted for employing diffusion Monte Carlo (DMC),[54] an atomistic simulation method capable of exactly sampling the ground state vibration wave function Ψ_0 for M*He$_n$ systems, to study the structure and energetics of the latter. Since the DMC methods have extensively been described in the literature, we restrict ourselves to providing only the details needed to understand our results and, refraining from a lengthy discussion, referring the interested reader to previously published material (*e.g.* see ref. 55).

Given the reasonably deep well present in the M*–He interaction potentials (that is, neglecting the repulsive $^2\Sigma^+$ states correlating with the atomic ^{2}P ones), we chose not to use any guiding wave function Ψ_T for directing the simulations to avoid any bias that may be introduced due to shortcomings of its form. As for the sampling algorithm, we employed the third order ''on the fly'' propagator previously developed[56] and that uses an intermediate half-step potential evaluation to extrapolate the branching weights to third order. A time step δt = 300 Hartree^{-1} was found to be sufficiently small to guarantee a small systematic bias for all clusters simulated when used in conjunction with a walker population weight of above 1000. Energies were computed using the simple potential estimator,[54] *i.e.* averaging the value of the interaction potential over the sampled configurations. The DMC algorithm was implemented to minimize the ''step to step'' stochastic error associated with the diffusion and branching steps.[57] Albeit more accurate options are available for unguided DMC,[58,59] we simply collected the configuration replicas (whose distribution is proportional to Ψ_0) sampled during the DMC simulation to obtain structural details of the systems investigated. This approach was previously found to generate a sufficient level of insight into reasonably structured systems.[60] Correlation between statistical samples was eliminated using the blocking method.[61]

3.2 Diatomics-in-Molecule (DIM) analytic potentials

Differently from the case of He clusters doped with metal atoms in a S-type ground state, the interaction potential for M*He$_n$ cannot, at least in principle, be written as a ''sum of pairwise interactions''. This is due to the strong anisotropic character of the many-body effects defining the orientation of the angular momentum projection axis that minimises the energy of the system. Since *ab initio* methods are far too expensive to be used for obtaining well converged DMC simulations, in this work we resort to the use of the Diatomics-in-Molecule approach originally developed by Ellison[35] (see ref. 62 for a more modern presentation including also a discussion on the *ab initio* and semi-empirical versions of the method). In this method, the total electronic Hamiltonian of a system is written as sum of mono- and di-atomic Hamiltonian operators, while the wave function is a linear combination of anti-symmetrized products of mono- and di-atomic diabatic terms.[62]

In the semi-empirical version of the DIM approach for M*He$_n$, only the antisymmetric products containing the ground state of the He atoms and one of the excited states of the metal atom are used to represent the total wave function. In this case, this is justified by the large energy difference between electronic states in M*He$_n$, as discussed in ref. 31 for Ca–Ar. Neglecting the indication of the ^{1}S configuration of the He(1s^2) atoms, we would represent such a product indicating only the angular momentum of the metal electronic state with the ket $|lm\rangle$. The contribution to a matrix element coming from any of the diatomic Hamiltonian operators is approximated using semi-empirical or, as in our case, with accurate pair interaction energies. In both cases, however, we usually know pair potential curves in the reference frame that uses the bond axis of each specific diatomic as a projection axis (*i.e.* each state correlates with a $|lm\rangle_M$ in a specific diatomic frame), while we would need to express them with respect to a common reference (*e.g.* the laboratory one). Indicating with $|lm\rangle_L$ the metal state in the laboratory frame, the diatomic matrix element between $|lm\rangle_L$ and $|lm'\rangle_L$ (notice that both states have the same l as no mixing between different angular momentum states is allowed in the DIM matrix) can be written as:

$$\begin{aligned}&{}_L\langle lm|\mathscr{H}_{MHe}|lm'\rangle_L\\&=\sum_{m_1m_1'}{}_L\langle lm\mid lm_1\rangle_{MM}\langle lm_1|\mathscr{H}_{MHe}|lm_1'\rangle_{MM}\langle lm_1'\mid lm'\rangle_L\end{aligned}\quad(1)$$

Since one writes the identity $\mathscr{I}=\sum_{m_1}|lm_1\rangle\langle lm_1|$ for a chosen total angular momentum l. Indicating as $\mathscr{R}^a(\alpha,\beta,\gamma)$ the active rotation operator (with the convention used by Sakurai[63] to define Euler angles) that re-orients the diatomic M–He from being aligned with the z-axis of the laboratory frame and having M in the origin to the more general orientation of its bond vector indicated by (α,β,γ), one has:

$$\mathscr{R}^a(\alpha,\beta,\gamma)|lm\rangle_L=|lm\rangle_M\quad(2)$$

or, substituting into eqn (1):

$$\begin{aligned}{}_L\langle lm|\mathscr{H}_{MHe}|lm'\rangle_L=\sum_{m_1m_1'}{}_L\langle lm|\mathscr{R}^a(\alpha,\beta,\gamma)|lm_1\rangle_{LM}\langle lm_1|\mathscr{H}_{MHe}|lm_1'\rangle_M\\\times{}_L\langle lm_1'|(\mathscr{R}^a(\alpha,\beta,\gamma))^\dagger|lm'\rangle_L\end{aligned}\quad(3)$$

The matrix elements ${}_L\langle lm|\mathscr{R}^a(\alpha,\beta,\gamma)|lm_1\rangle_L$ for the rotation are the coefficient $\mathbf{D}^l_{mm_1}(\alpha,\beta,\gamma)$ of the basis element $|lm\rangle_L$ in the linear combination that represents the effect of the rotation $\mathscr{R}^a(\alpha,\beta,\gamma)$ on $|lm_1\rangle_L$ and are given in ref. 63 and 64.† Since rotations are unitary transformations, the matrix composed of the elements ${}_L\langle lm_1'|\mathscr{R}^a(\alpha,\beta,\gamma)^\dagger|lm'\rangle_L$ is the inverse of $\mathbf{D}^l_{mm_1}(\alpha,\beta,\gamma)$. The matrix $\mathbf{H}^{MHe}_{mm_1}={}_M\langle lm_1|\mathscr{H}_{MHe}|lm_1'\rangle_M$ expressed in the diatomic molecular frame is diagonal and would represent the diabatic interaction between the 1s^2 He and the $|lm\rangle_M$ state of the metal as

† The Wigner small $\mathbf{d}^l_{mm_1}(\alpha,\beta,\gamma)$ matrix in ref. 64 contains an error in the $\mathbf{d}^l_{1,-1}(\alpha,\beta,\gamma)$ element, which should be $-\frac{1}{2}(2\cos^2\beta-\cos\beta-1)$.

a function of their distance. It is customary to substitute such diagonal diabatic interactions with the adiabatic potential energy curves associated asymptotically with each of the projection quantum numbers m. Thus, for a P state of the metal, one would associate the two degenerate Π diatomic state with $m = -1,1$, and the Σ diatomic state with $m = 0$. For a D state of the metal, one would extend such a prescription with the association of the degenerate Δ diatomic states to $m = -2,2$. Notice, however, that the diagonalization of the matrices obtained using the adiabatic potential curves provides one with states that are eigenfunctions of both the unperturbed atomic Hamiltonian as well as the He-related and spin–orbit perturbation, thus breaking the degenerate nature of the original P or D manifolds. Nevertheless, it is worth pointing out that a diabatic approach (as the one employed by Heitz *et al.*[31]) would allow an improved accuracy, especially when configurational mixing ought to be expected (*vide infra* Sections in 4.2); this is because the DIM approach relies on the assumption that diatomic states maintain the same configurational character. Indeed, mixing could lead to the non-adiabatic transitions that are often invoked to explain excited state depopulation or fluorescence line disappearance, and the coupling elements needed for the dynamical simulations of such processes are more easily obtained starting from a diabatic picture rather than an adiabatic one.

The matrix $\mathbf{D}\mathbf{H}^{\mathrm{MHe}}\mathbf{D}^{\dagger}$ providing the contribution for a specific diatomic M–He pair with the metal in a P state has been given previously as a function of α and β, the latter representing the angles giving, respectively, ϕ and θ of the polar coordinates

$$\begin{aligned}
\mathbf{M}_{11} &= \frac{1}{8}\big(V_\Delta + 6V_\Delta\cos^2\beta + V_\Delta\cos^4\beta + 4V_\Pi\sin^2\beta \\
&\quad + 3V_\Sigma\sin^4\beta + V_\Pi\sin^2(2\beta)\big) \\
\mathbf{M}_{12} &= \frac{\mathrm{e}^{-i\alpha}}{4}\cos\beta\sin\beta\big((V_\Delta - 4V_\Pi)\cos^2\beta + 3\big(V_\Delta - V_\Sigma\sin^2\beta\big)\big) \\
\mathbf{M}_{13} &= \frac{\mathrm{e}^{-2i\alpha}}{8}\sqrt{\frac{3}{2}}(3V_\Delta - 4V_\Pi + V_\Sigma + (V_\Delta - 4V_\Pi + 3V_\Sigma)\cos(2\beta))\sin^2\beta \\
\mathbf{M}_{14} &= \frac{\mathrm{e}^{-3i\alpha}}{4}(V_\Delta - 4V_\Pi + 3V_\Sigma)\cos\beta\sin^3\beta \\
\mathbf{M}_{15} &= \frac{\mathrm{e}^{-4i\alpha}}{8}(V_\Delta - 4V_\Pi + 3V_\Sigma)\sin^4\beta \\
\mathbf{M}_{22} &= \frac{1}{8}\big(4V_\Pi - 12V_\Pi\cos^2\beta + 16V_\Pi\cos^4\beta + 4V_\Delta\sin^2\beta \\
&\quad + V_\Delta\sin^2(2\beta) + 3V_\Sigma\sin^2(2\beta)\big) \\
\mathbf{M}_{23} &= -\frac{\mathrm{e}^{-i\alpha}}{8}\sqrt{\frac{3}{2}}(-V_\Delta + V_\Sigma + (V_\Delta - 4V_\Pi + 3V_\Sigma)\cos(2\beta))\sin(2\beta) \\
\mathbf{M}_{24} &= \frac{\mathrm{e}^{-2i\alpha}}{4}\big(V_\Delta + 2V_\Pi - 3V_\Sigma - (V_\Delta - 4V_\Pi + 3V_\Sigma)\cos(2\beta)\big)\sin^2\beta \\
\mathbf{M}_{25} &= -\frac{\mathrm{e}^{-3i\alpha}}{4}(V_\Delta - 4V_\Pi + 3V_\Sigma)\cos\beta\sin^3\beta \\
\mathbf{M}_{33} &= \frac{1}{4}\Big(V_\Sigma\big(1 - 3\cos^2\beta\big)^2 + 3V_\Delta\sin^4\beta + 3V_\Pi\sin^2(2\beta)\Big) \\
\mathbf{M}_{34} &= \frac{\mathrm{e}^{-i\alpha}}{8}\sqrt{\frac{3}{2}}(-V_\Delta + V_\Sigma + (V_\Delta - 4V_\Pi + 3V_\Sigma)\cos(2\beta))\sin(2\beta) \\
\mathbf{M}_{35} &= \frac{\mathrm{e}^{-2i\alpha}}{8}\sqrt{\frac{3}{2}}\big(3V_\Delta - 4V_\Pi + V_\Sigma + (V_\Delta - 4V_\Pi + 3V_\Sigma)\cos(2\beta)\big)\sin^2\beta \\
\mathbf{M}_{44} &= \frac{1}{8}\big(4V_\Pi - 12V_\Pi\cos^2\beta + 16V_\Pi\cos^4\beta + 4V_\Delta\sin^2\beta \\
&\quad + V_\Delta\sin^2(2\beta) + 3V_\Sigma\sin^2(2\beta)\big) \\
\mathbf{M}_{45} &= \frac{\mathrm{e}^{-i\alpha}}{4}\cos\beta\sin\beta\big(-3V_\Delta - (V_\Delta - 4V_\Pi)\cos^2\beta + 3V_\Sigma\sin^2\beta\big) \\
\mathbf{M}_{55} &= \frac{1}{8}\big(V_\Delta + 6V_\Delta\cos^2\beta + V_\Delta\cos^4\beta + 4V_\Pi\sin^2\beta \\
&\quad + 3V_\Sigma\sin^4\beta + V_\Pi\sin^2(2\beta)\big)
\end{aligned} \tag{4}$$

$(r\cos\phi\sin\theta, r\sin\phi\sin\theta, r\cos\theta)$ of the He atom with respect to the metal.[65] The analytical representation of a diatomic contribution when the metal is in a D state is given in this work as:with the usual Hermitian condition that $\mathbf{M}_{ji} = \mathbf{M}_{ij}^{*}$ for the elements $\mathbf{M}_{ji}$ below the diagonal (*i.e.* $j > i$) and assuming the ordering $m = 2 \rightarrow i = 1$, $m = 1 \rightarrow i = 2$, $m = 0 \rightarrow i = 3$, $m = -1 \rightarrow i = 4$, $m = -2 \rightarrow i = 5$ and correspondingly for the index j.

For the coinage metals, the spin–orbit coupling for the P and D states is sufficiently large to require it to be included as an important contribution to the energetics of the doped clusters. In particular, we employed an atoms-in-molecule approach, assuming a constant value for the spin–orbit coupling constant a although it should be formally dependent on the cluster geometry. As the correct treatment of the spin–orbit coupling requires the $|lm\rangle$ states to be multiplied by spin functions $|\sigma\rangle$ (that is, $|\alpha\rangle$ and $|\beta\rangle$ for ^{2}P and ^{2}D states), the complete interaction matrix including the spin–orbit contributions is twice as large as the $\mathbf{M}$ matrix (see eqn (4)) when expressed in the $|lm\rangle_{\mathrm{L}} \otimes |\sigma\rangle$ basis set. The complete Hamilton matrix for an atom in a ^{2}P state descending from a p^1 configuration has been given previously.[39] For the ^{2}D state descending from the $(n-1)d^9ns^2$ configuration of Cu, Ag and Au, the matrix can be easily derived from the matrix $\mathbf{M}$ if one maintains the ordering given above for m and uses the basis elements containing the spin function $|\alpha\rangle$ as the first five elements. With such ordering, the matrix for the spin–orbit coupling interaction in the $|lm\rangle_{\mathrm{L}} \otimes |\sigma\rangle$ basis set can be computed using the formula

$$\begin{aligned}
&\langle m_k\sigma_k|\hat{h}_{\mathrm{SO}}|m_j\sigma_j\rangle \\
&= \frac{a}{2}\sqrt{l(l+1) - m_j(m_j+1)}\sqrt{s(s+1) - \sigma_j(\sigma_j - 1)}\,\delta_{m_k,m_j+1}\delta_{\sigma_k,\sigma_j-1} \\
&+ \frac{a}{2}\sqrt{l(l+1) - m_j(m_j-1)}\sqrt{s(s+1) - \sigma_j(\sigma_j + 1)}\,\delta_{m_k,m_j-1}\delta_{\sigma_k,\sigma_j+1}
\end{aligned} \tag{5}$$

with $\hat{h}_{\mathrm{SO}}$ being the spin–orbit interaction operator, l and s the orbital (*i.e.* $l = 2$ for the D state) and spin (*i.e.* $s = 1/2$ for the doublet state) angular momenta, and m and σ, respectively,

their projection along the z-axis. The explicit form of the spin–orbit matrix obtained with eqn (5) is:

$$\begin{pmatrix} m,\sigma & 2\alpha & 1\alpha & 0\alpha & -1\alpha & -2\alpha & 2\beta & 1\beta & 0\beta & -1\beta & -2\beta \\ 2\alpha & -a & 0 & 0 & 0 & 0 & 0 & 0 & 0 & 0 & 0 \\ 1\alpha & 0 & -a/2 & 0 & 0 & 0 & -a & 0 & 0 & 0 & 0 \\ 0\alpha & 0 & 0 & 0 & 0 & 0 & 0 & \sqrt{\frac{3}{2}}a & 0 & 0 & 0 \\ -1\alpha & 0 & 0 & 0 & a/2 & 0 & 0 & 0 & \sqrt{\frac{3}{2}}a & 0 & 0 \\ -2\alpha & 0 & 0 & 0 & 0 & a & 0 & 0 & 0 & a & 0 \\ 2\beta & 0 & a & 0 & 0 & 0 & a & 0 & 0 & 0 & 0 \\ 1\beta & 0 & 0 & \sqrt{\frac{3}{2}}a & 0 & 0 & 0 & a/2 & 0 & 0 & 0 \\ 0\beta & 0 & 0 & 0 & \sqrt{\frac{3}{2}}a & 0 & 0 & 0 & 0 & 0 & 0 \\ -1\beta & 0 & 0 & 0 & 0 & a & 0 & 0 & 0 & -a/2 & 0 \\ -2\beta & 0 & 0 & 0 & 0 & 0 & a & 0 & 0 & 0 & -a \end{pmatrix} \quad (6)$$

which has a six-fold degenerate eigenvalue equal to $-a$ and corresponding to a state with a total angular momentum $J = 5/2$, and a four-fold degenerate one with value $3a/2$ that corresponds to the states with total angular momentum $J = 3/2$. From this results, one obtains that $\Delta E_{SO} = E_{3/2} - E_{5/2} = 5a/2$, or $a = 2\Delta E_{SO}/5$. In the following, we used ΔE_{SO} = 248.38, 920.66 and 3815.622 cm^{-1} for the ^{2}P state of, respectively, Cu, Ag, and Au; in the same order of metals, ΔE_{SO} = 2042.858, 4471.928, and 12274.014 cm^{-1} for the ^{2}D state.

4 Simulation results

In the present section, we shall discuss the results of the DMC simulations on the M*(^{2}L)He$_n$ systems, with L = P, D. In doing this, we would proceed discussing the results for the ^{2}P states at first, which are of relevance for the formation of exciplexes following the ^{2}P ← ^{2}S UV excitation of a coinage metal that generates the D1 and D2 bands. Subsequently, the case of the ^{2}D states is presented, discussing their link to photo-excitation experiments in bulk and vapour helium.

4.1 ^{2}P states

As of relevance for the ensuing discussion, Fig. 2 shows the interaction potentials for the three coinage metals correlating with the atomic spin–orbit coupled states $^2P_{1/2}$ ($^2\Pi_{1/2}$) and $^2P_{3/2}$ ($^2\Pi_{3/2}$ and $^2\Sigma^+$).

Owing to the difference shown in Fig. 1 for the $^2\Pi$ and $^2\Sigma$ interaction potentials correlating with the ^{2}P state of the coinage metals and to the different magnitude of the spin–orbit interactions, stark qualitative differences between the metals emerge from Fig. 2. In particular, we notice that the $^2\Pi_{1/2}$ potential becomes less attractive (or more repulsive) upon increasing the atomic number, the potential for Au being markedly repulsive over the complete range of distance investigated. The quantity ΔE_{SO} plays an important role in defining the trend described, as it is directly related to the off-diagonal (*i.e.* mixing) element between the $^2\Pi$ and $^2\Sigma$ curves $\left(\mathbf{M}_{\Pi,\Sigma} = \frac{\sqrt{2}}{3}\Delta E_{SO}\right)$ that generate the $^2\Pi_{1/2}$ and $^2\Sigma^+$ curves[27] for M*(^{2}P)He. In particular, the larger the value of the spin–orbit splitting, the larger the distance range over which it is possible to mix the repulsive $^2\Sigma$ state with the attractive $^2\Pi$ one in the linear combination that defines the $^2\Pi_{1/2}$ potential. For Au, the mixing is also facilitated by a weaker interaction with helium in the $^2\Pi$ state compared with the remaining metals, as indicated in Section 2. In the case of Cu, the deep potential well for the $^2\Pi$ Cu–He state and the comparatively small spin–orbit constant induce only a small entrance barrier ($\sim$30 cm^{-1}) in the $^2\Pi_{1/2}$ potential and a weak raise of the well bottom compared to the original $^2\Pi$ potential. No effects other than uniformly raising the $^2\Pi$ curve are induced in the $^2\Pi_{3/2}$ potential. Albeit more marked, qualitatively similar effects are present in the Ag case, the curve minimum at around 2.5 Å becomes nearly degenerate (roughly 10.2 cm^{-1} below) with the dissociated fragments $^2P_{1/2}$ Ag and He.

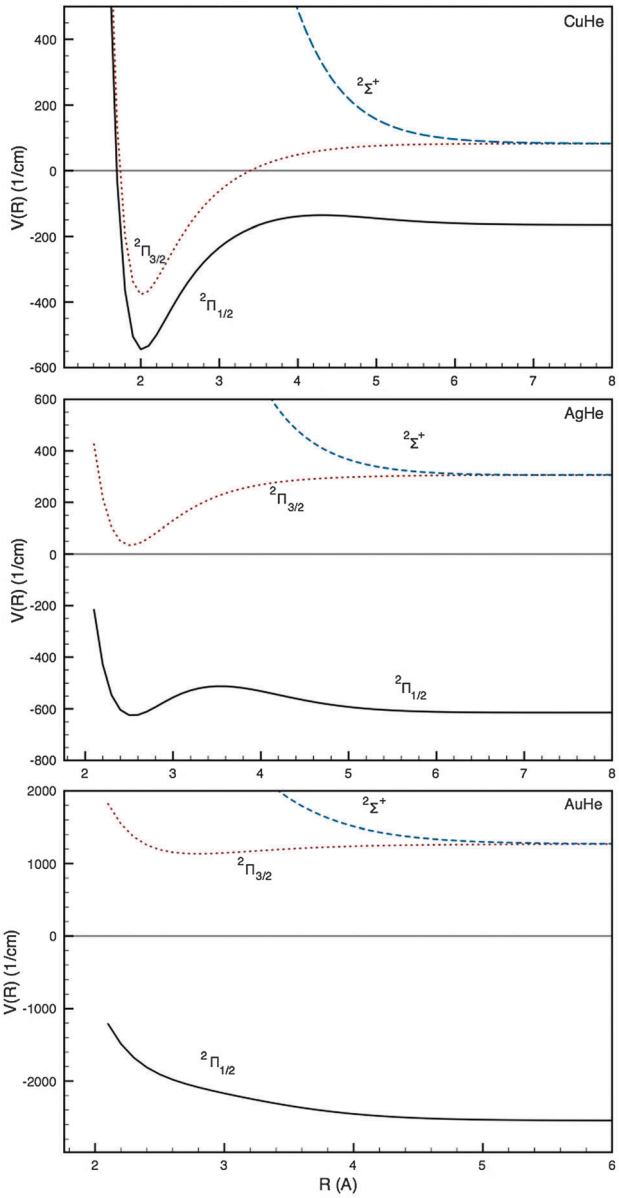

Fig. 2 M*(^{2}P)–He pair potentials including spin–orbit coupling interaction. The zero of the energy is chosen as the energy of the spin–orbit averaged M*(^{2}P) plus He energies. Energies in cm^{-1}, distances in Å.

From Fig. 2, it is also apparent that the highest lying pair of degenerate eigenvalues obtained diagonalising **M** produces always a repulsive curve, as it was expected since it should correlate the most with the repulsive $^2\Sigma$ spin–orbit averaged state. As previous works[66] have shown that this repulsive character translates into the many-body cases, we avoided any further study on such eigenvalues. Instead, we concentrated on investigating the energetics and structural features of the first and second excited states for Cu and Ag, and only of the second state of Au given the repulsive nature of its lowest one. In this respect, it is also interesting to notice that the $^2\Pi_{1/2}$ potential for Au could be thought as a weighted average between the $^2\Sigma$ and $^2\Pi$ states, with coefficients being substantially defined by the coefficients of the linear combination representing the $^2P_{1/2}$ state in terms of the $|1m\rangle \otimes |\sigma\rangle$ basis set. This is due to the higher magnitude of the spin–orbit coupling compared with the well depth (*i.e.* to the weakly perturbing action of the M–He interaction on the S–O coupled states). Thus, the $^2\Sigma$ potential is capable of "washing away" the attractive well of the $^2\Pi$ state, generating a totally repulsive interaction due to the earlier and rapid onset of its repulsive wall compared with the attractive well of $^2\Pi$.

4.1.1 Cu. DMC binding energy results for the two lowest eigenstates of Cu*(^{2}P)He$_n$ are given in Table 2, together with the negative of the He evaporation energies defined as:

$$-\Delta_0(n) = \frac{E_0(n) - E_0(m)}{n - m} \qquad (7)$$

with m being the largest integer for which $n > m$.

As indicated by the results in Table 2, the potential for the lowest state is capable of binding up to 5 He atoms, a sixth one dissociating quickly from the cluster as the DMC simulation progresses despite an initially low value of the average potential for the starting structure. In this respect, it is noticeable that $\Delta_0{}^1$ substantially decreases upon increasing n from 4 to 5, indicating for n = 5 a nearly saturated binding capability for Cu in this state. Given the Cu–He equilibrium distance for the $^2\Pi$ or $^2\Pi_{1/2}$ states (see Fig. 1 and 2), it seems to be unlikely that the whole "surface" of Cu is completely covered by only 5 He atoms, thus suggesting a toroidal disposition for the He atoms around the "waist" (*i.e.* the nodal plane) of the $^2P_{1/2}$ state. To show that this is just the case, Fig. 3 shows a typical structure for Cu*(^{2}P)He$_5$ sampled during the DMC simulation.

The structure shown in Fig. 3 for Cu*($^2P_{1/2}$)He$_5$ is clearly reminiscent of the structure evidenced for the lowest excited state of Li*(^{2}P)He$_5$ and Na*(^{2}P)He$_5$,[30] K*(^{2}P)He$_6$,[32] and Rb*(^{2}P)He$_7$.[28] In other words, the structure of these clusters is decided by a competition between the strong attraction of a He atom from the unscreened cationic Cu$^+$ core along the nodal plane and the excluded volume of the He atoms.

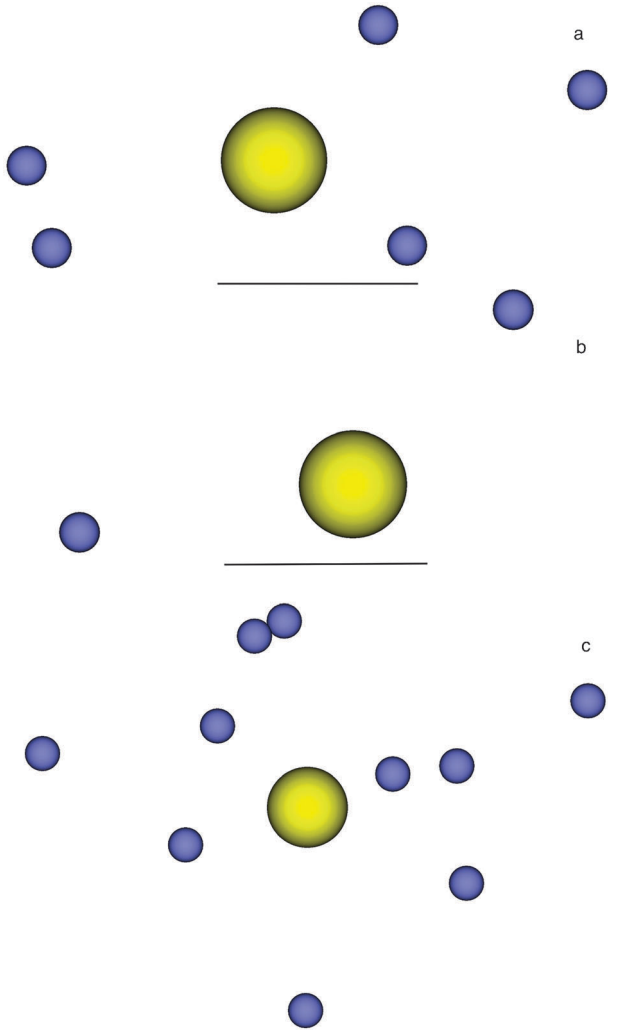

Fig. 3 Structure of a few M*(^{2}P)He$_n$ and M*(^{2}D)He$_n$ complexes collected during the DMC sampling of Ψ_0. (a) Cu*($^2P_{1/2}$)He$_5$; (b) Cu*($^2P_{3/2}$)He$_2$; (c) Cu*($^2D_{5/2}$)He$_{10}$, the first eigenvalue of the DIM matrix.

Turning to the exciplexes formed when Cu* correlates asymptotically with the $^2P_{3/2}$ state, we found that no more than two He atoms can be strongly bound to the metal (see Table 2 and Fig. 3 for its structure). In these cases, the total binding energy for the two stable species is larger than the corresponding systems containing Cu*($^2P_{1/2}$), owing to a substantially larger binding energy of the first He atom to the metal centre in the $^2P_{3/2}$ state. The substantial stability of Cu*($^2P_{3/2}$)-He$_n$ for n = 1 and 2 parallels what previously suggested more generally for alkali-type metals in a ^{2}P state,[67] Ag,[1,27] K,[32] Rb[6,29] and Cs,[4] thus supporting some of the experimental assignments.[9] Broadly speaking, the difference between the exciplexes formed with a large a (*i.e.* heavy) metal atom in the $^2P_{3/2}$ state and the ones built with the dopant in the $^2P_{1/2}$ is due to the fact

Table 2 DMC binding energy $E_0^\lambda(n)$ and negative evaporation energy $\Delta_0^\lambda(n)$ for the two lowest states (λ = 1,2) of Cu*(^{2}P)He$_n$

n	$E_0^1(n)^a$	$\Delta_0^1(n)^a$	$E_0^2(n)^a$	$\Delta_0^2(n)^a$
1	289.57		369.9	
2	592.1	−302.4	602.7	−232.8
3	864.7	−272.7		
4	1120.7	−255.9		
5	1177.0	−56.7		

[a] Energies in cm^{-1}. The standard error of mean values is roughly one unit of the last decimal digit shown.

that in the wave function of the former the node lies on a line (the quantisation axis), whereas it is on a plane in the latter case.[67] The preferential bonding zones for He atoms (*i.e.* the region where they can feel the Coulomb interaction with the unscreened core due to a reduced electron density) sit along the quantisation axis, thus forcing a nearly linear arrangement for these species. It is also noteworthy that no entrance barrier to the binding zone was found for the two He atoms (data not shown), a finding that agrees nicely with what previously indicated for K,[32] Rb[6] and Cs,[4] and that is clearly relevant for the possible post-excitation generation of $Cu^*(^2P_{3/2})He_2$.

As a final comment, one which is also generally valid for *all* the stable exciplexes, it is worth remembering that it has already been shown that species such as $Cu^*(^2P_{1/2})He_n$ and $Cu^*(^2P_{3/2})He_n$ are capable of binding additional He atoms, thus forming larger aggregates than the ones studied here.[28,29] This is substantially due to the juxtaposition of two known facts for He_n: first, the fact that He_2 is stable despite the weak potential interaction and its light reduced mass; second, the fact that when an M*He moiety is strongly bound, it basically acts as if it was a single He with a heavier mass. Thus, the results shown in Table 2 indicate that the dissociation of the sixth He atom from $Cu^*(^2P_{1/2})He_5$ and the third from $Cu^*(^2P_{3/2})He_3$ is due to some inefficiency of our algorithms when it comes to simulating aggregates kept together by weak interactions such as the He–He ones. Wishing to correct for this deficiency,[28] it would be an easy task to employ a guiding function Ψ_T for these systems as previously done in the case of molecular dopants;[68] at the moment, we consider this task outside the aim of this work, which mainly focuses on studying the exciplex ''core'' that may be formed following spectroscopical excitation and subsequent relaxation.

4.1.2 Ag. The presence of a well in the $^2\Pi_{1/2}$ state of Ag*–He (see Fig. 2) at around 2.5 Å with a depth of roughly 10.2 cm^{-1} with respect to the asymptotic fragments suggests the possible stability of the excimer. It must be noticed, however, that the potential well is rather narrow (width $\sim$1.25 Å), requiring the He atoms to sustain a tight confinement in order to form an aggregate. Thus, the potential may turn out to be unable to bind even a single rare gas atom, as the kinetic vibrational energy due to the confinement makes it possible for a dimer prepared with He atoms inside the well to ''leak-out'' through the exit barrier.

DMC simulations started with the dimer at the equilibrium distance indeed rapidly led to its dissociation, the quantum effect winning over the confining potential. To make sure of the robustness of the result, we also solved the Schroedinger equation with the previously used grid-based method[39] and found it always with energy slightly above dissociation and tending to the asymptotic limit upon converging the grid parameters. Attempts of characterising possible s-wave resonances were also unfruitful, the computed phase shift behaving monotonously over an energy range covering the possibility of classically surmounting the barrier.

Given this evidence, we avoided to run any simulation on the first excited state of the ^{2}P manifold for $AgHe_n$. It must be noted, however, that our results are at variance with the outcome of a previous dynamical study[33] following the post-excitation evolution of $AgHe_n$ clusters; this showed the formation of stable exciplexes with Ag in the $^2P_{1/2}$ state and characterised by the typical ''He belt'' structure (*vide* Section 2). However, the semi-classical trajectories in ref. 33 were based on curves[27] that have been suggested to overbind the dimer,[34] a feature that may be expected to bias the results favouring the formation of exciplexes. Given the fact that the indication of a possible direct formation of exciplexes from vertical electronic excitation provided by previous DMC calculations on $AgHe_n$[39] employing the potentials in ref. 27 has been recently revised by similar calculations carried out with the most modern potential curves,[34] it is sensible to expect a different outcome also for the post-excitation dynamics.

Notice that the lack of stable $AgHe_n$ aggregates when the metal is in the $^2P_{1/2}$ state provides an *a posteriori* justification for, first, the lack of $^2P_{1/2}$ exciplex signatures even in liquid He[1] and, second, for the experimental observation that silver tends to be expelled from He droplets[36] when converted into the $^2P_{1/2}$ state by, for instance, non-adiabatic transition following excitation of the D2 line. Ag is also expected to be expelled from clusters when excited in the third state of the same manifold, as the $^2\Sigma^+$ potential for AgHe appears to be repulsive over the whole range of distances.

Focusing on the second excited state of the ^{2}P manifold of Ag, Table 3 gives the same quantity provided above for $CuHe_n$.

Similar to that evidenced for Cu, the PES of the second excited state of $Ag^*(^2P)He_n$ allows only two He atoms to strongly bind to the metal atom. Snapshots extracted during the DMC sampling showed that $Ag^*(^2P)He_2$ has a linear (average) geometry similar to the case of Cu (see panel b of Fig. 3 for a snapshot view). Moreover, there are no exit barriers for the He atoms on both sides, supporting the possibility that both the dimer and the trimer can be formed following photo-excitation. Indeed, this outcome was evidenced already monitoring UV fluorescence of Ag in surperfluid liquid helium.[1] The theoretical modelling of the post-excitation dynamics in ref. 33 also pointed toward this possibility, although it is important to remember that the expected overbinding nature of the potential employed is likely to increase the silver ''catchment basin'' for He companions.

4.1.3 Au. As discussed at the beginning of Section 4.1, the lowest state of the ^{2}P manifold for Au is repulsive even when a single He atom is present due to the strong mixing between the $^2\Pi$ and $^2\Sigma$ states induced by the large spin–orbit constant. Thus, we dispatched with studying this state as it is unlikely to produce any non-trivial result.

Table 3 DMC binding energy $E_0^2(n)$ and negative evaporation energy $\Delta_0^2(n)$ for the second state (λ = 2) of $Ag^*(^2P)He_n$

n	$E_0^2(n)^a$	$\Delta_0^2(n)^a$
1	211.55	
2	354.7	−143.2

[a] Energies in cm^{-1}. The standard error of mean values is roughly one unit of the last decimal digit shown.

Table 4 DMC binding energy $E_0^{\lambda}(n)$ and negative evaporation energy $\Delta_0^{\lambda}(n)$ for the second state (λ = 2) of Au*(^{2}P)He$_n$

n	$E_0^2(n)^a$	$\Delta_0^2(n)^a$
1	98.46	
2	150.2	−51.7

[a] Energies in cm^{-1}. The standard error of mean values is roughly one unit of the last decimal digit shown.

With respect to the second excited state of the ^{2}P manifold, Table 4 shows the energy results for the only two stable aggregates found. DMC sampled configurations gave geometries similar to what found for the other two metals in this electronic state. To the best of our knowledge, no previous report of the stability for this species is available in the literature. It is worth noting that there is a trend of decreasing binding energy for M(^{2}P$_{3/2}$)He$_n$ (n = 1 and 2) along the series Cu, Ag and Au. This closely follows the decrease in interaction strength in the $^2\Pi$ states of M–He upon increasing the atomic number already mentioned in Section 2.

4.2 ^{2}D states

As indicated previously in Section 2, the potential curves for M*(^{2}D)–He present a very weak dependency on both the metal atom M and the projection of the angular momentum (*i.e.* Σ, Π and Δ) on the bond axis. This is largely due to the screening by the external ns^2 electrons of the d hole created as a consequence of the electronic excitation. The orientational effects are thus reduced to the point that the well depths of potentials deriving from different angular momenta differ, at most, by 1.2 cm^{-1} for Cu, an interpretation supported by the close equilibrium distance in the M*(^{2}D)–He curves and in the ground state interactions. Specifically, we highlight a small contraction ($\sim$−0.2 Å) with respect to the ground state for Cu or Ag, and a slight expansion ($\sim$0.2 Å) for Au.

From the energetic standpoint, it is noteworthy that the interaction well depth for the ^{2}D states of all the metals spans the range $\sim$11–18 cm^{-1}; the interaction is therefore to be considered weak with respect to the spin–orbit coupling in these states (ΔE_{SO} = 2042.858, 4471.928, and 12274.014 cm^{-1} for Cu, Ag and Au, respectively) and expected to play only the role of a weak perturbation of the S–O coupled states. This observation has indeed a profound consequence on the dependency of exciplex structural details upon the specific electronic state correlating with the manifold defined by the $(n-1)d^9ns^2$ ^{2}D configuration, as the total angular momentum J and its projection m_J represent good quantum numbers. With the relative weights of the Σ, Π and Δ potential giving the interaction surface for a specific electronic state $|Jm_J\rangle$ coming directly from averaging **M** over the linear combination of $|lm\rangle$ defining it, the similarity between the Σ, Π and Δ curves produces a nearly isotropic interaction for the He atoms due to the unitary nature of the rotation matrix. In turn, these results indicate that the perturbation introduced into the energetics of the $|J,m_J\rangle$ states does not depend strongly on the specific J or m_J chosen. A similar conclusion can be reached starting from the analysis carried out by Danilychev and Apkarian[69] based on the classical decomposition of the interaction anisotropy in terms of Legendre polynomials.

As a consequence of the above scrutiny, one would not expect any major differences between species containing different metals due to the differences in the interaction energy alone. An additional consequence is the expectation of a nearly spherical interaction surface whatever the eigenvalue of **M**, with only minor changes between different states and for different metals. So, there is in principle no need to refer to spin–orbit coupled dimer surfaces as in Fig. 2 for the ^{2}P states, and we thus avoid to present them for the sake of brevity. Of course, this is at variance with what found earlier for the ^{2}P states, the qualitative features of the spin–orbit coupled energy surfaces hinging on that manifold being strongly dependent on both the metal–helium interaction and the spin–orbit constant.

The analysis carried out above is already sufficient to rationalise a few of the details in the laser ablation fluorescence studies carried out on Cu and Au in solid and liquid ^{4}He.[8,9] First, the very weak shift found for the fluorescence lines related to the decay of the ^{2}D$_{3/2,5/2}$ states into the ground ^{2}S is fully supported by the weak M–He interaction of both configurations, and their similar equilibrium distances and well widths. Second, the long decay lifetime found for the ^{2}D$_{3/2,5/2}$ states in solid ^{4}He is justified by the minor differences between the Σ, Π and Δ potentials, the net effect of which would be to maintain the surrounding of the excited atom spherical. This effect ought to be expected to reduce also the likelihood of a local (*e.g.* dipolar) distortion sufficiently strong to induce a coupling between the M excited and ground states. Subtler interpretation, perhaps requiring also using the data for the ^{2}P states, will be discussed in the ensuing presentation of the DMC results on the exciplexes formed by M*(^{2}D).

4.2.1 Cu. Table 5 provides the DMC results for both $E_0^{\lambda}(n)$ and $\Delta_0^{\lambda}(n)$ computed for the first, third and fifth energy level of Cu*(^{2}D)He$_n$. As one can notice, the binding energies for the clusters is much smaller than the one for Cu*(^{2}P)He$_n$, clearly owing to the weaker interaction between copper in the ^{2}D state and He. Also, it appears that our expectation of a very similar behaviour for *all* the energy levels is largely confirmed by the results. Noticeably, the nearly spherical symmetry of the interaction potentials allows Cu*(^{2}D) to bind up to 10 He atoms in

Table 5 DMC binding energy $E_0^{\lambda}(n)$ and negative evaporation energy $\Delta_0^{\lambda}(n)$ for the first, third and fifth states (λ = 1,3,5) of Cu*(^{2}D)He$_n$

n	$E_0^1(n)^a$	$\Delta_0^1(n)^a$	$E_0^3(n)^a$	$\Delta_0^3(n)^a$	$E_0^5(n)^a$	$\Delta_0^5(n)^a$
1	7.28		6.71		6.18	
2	14.52	−7.24	13.41	−6.69	12.68	−6.49
3	21.80	−7.28	20.39	−6.98	19.44	−6.76
4	29.17	−7.37	27.48	−7.08	26.36	−6.92
5	36.61	−7.44	34.69	−7.21	33.47	−7.10
6	44.1	−7.5	42.01	−7.3	40.69	−7.23
8	59.3	−7.6	56.53	−7.2	55.0	−7.1
10	74.2	−7.4	71.34	−7.4	69.7	−7.4

[a] Energies in cm^{-1}. The standard error of mean values is roughly one unit of the last decimal digit shown.

its first shell. Panel (c) in Fig. 3 shows a uniform coverage of the metal in Cu*(^{2}D)He$_{10}$, an interpretation in good agreement with the similar He evaporation energies $\Delta_0^{\lambda}(n)$ as a function of n. In fact, the latter quantity is usually sensitive to the local environment[34] and it is expected to decrease sharply upon completion of the first solvation shell. As suggested at the beginning of Section 4.2, the low DMC binding energies for the ^{2}D copper exciplexes agree nicely with the very small shifts found experimentally for the $^2D_{5/2,3/2} \rightarrow {}^2$S fluorescence.[9]

Angular He–Cu–He distributions (not shown) indicate a nearly spherical helium density around ^{2}D Cu, a fact that allows us also to provide support for the suggested mechanism that permits the ^{2}P manifold depopulation into the ^{2}D one with no emission.[9] In this respect, we begin by noticing that the stabilisation afforded by the $^2P_{1/2,3/2}$ states of Cu when binding He atoms is not sufficient to lower their energy to a level close to the D states. Instead, the ring of He atoms found in Cu*($^2P_{1/2}$)-He$_5$ at a distance of roughly 2.25 Å from the copper (see Fig. 3 and 4) would raise the energy of the ^{2}D states by a rough average of 3000 cm^{-1} per He atom with respect to the dissociated fragments as estimated from our Σ, Π and Δ potentials. In turn, this means that the He ring in Cu*($^2P_{1/2}$)He$_5$ should be expected to increase the energy of the D states at least 15 000 cm^{-1} above its asymptotic form. With the average energy gap between the D and P manifolds being roughly 18 000 cm^{-1} and the stabilisation due to the formation of the exciplex being ~1177 cm^{-1}, quantum fluctuation of the He ring could easily bring the potential curve for the D state and the energy of the exciplex itself into a situation of near degeneracy. Albeit not sufficient on its own, the condition of near degeneracy facilitates the non-adiabatic crossing from one state to the other, the population of the lower D states, and hence the appearance of the fluorescence lines at 755 and 893 nm.

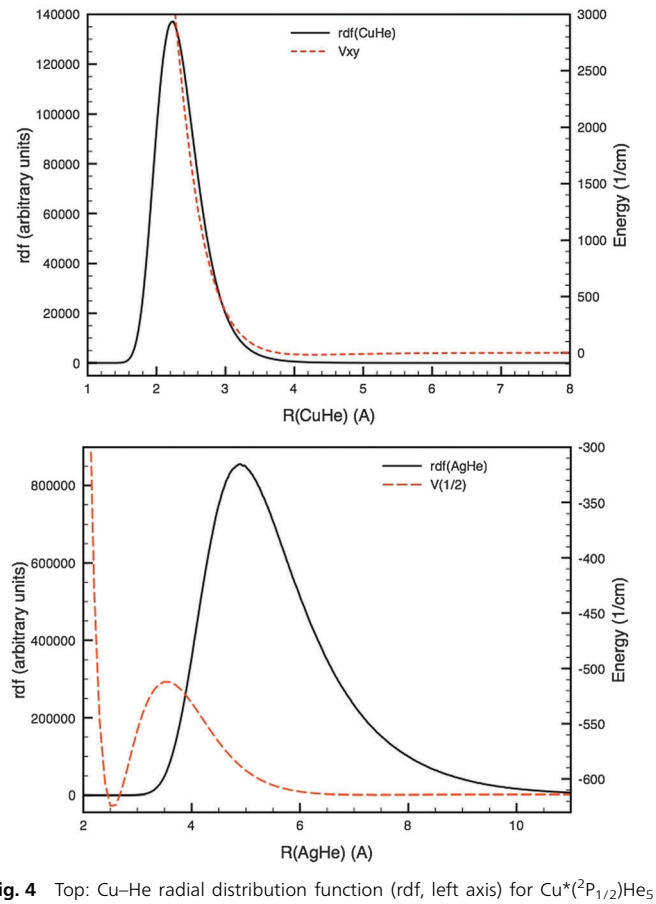

Fig. 4 Top: Cu–He radial distribution function (rdf, left axis) for Cu*($^2P_{1/2}$)He$_5$ and $V_{xy} = V_\Delta$ interaction potential (right axis) for Cu*(^{2}D)–He. Bottom: Ag–He radial distribution function (rdf, left axis) for Ag*($^2D_{5/2}$)He$_{10}$ and $V(1/2) = V_{\Pi_{1/2}}$ interaction potential (right axis) for Ag*(^{2}P)–He. Energies in cm^{-1}, distances in Å.

Table 6 DMC binding energy $E_0^{\lambda}(n)$ and negative evaporation energy $\Delta_0^{\lambda}(n)$ for the first, third and fifth states (λ = 1,3,5) of Ag*(^{2}D)He$_n$

n	$E_0^1(n)^a$	$\Delta_0^1(n)^a$	$E_0^3(n)^a$	$\Delta_0^3(n)^a$	$E_0^5(n)^a$	$\Delta_0^5(n)^a$
1	7.37		5.98		6.30	
2	14.50	−7.13	12.32	−6.34	12.91	−6.61
3	21.79	−7.29	19.01	−6.68	19.72	−6.81
4	29.15	−7.36	25.93	−6.91	26.79	−7.08
5	36.33	−7.18	32.89	−6.96	33.32	−6.53
6	43.8	−7.5	39.94	−7.05	40.25	−6.93
8	58.6	−7.4	53.8	−6.9	54.6	−7.2
10	72.9	−7.1	67.9	−7.1	68.2	−6.8

^{a} Energies in cm^{-1}. The standard error of mean values is roughly one unit of the last decimal digit shown.

4.2.2 Ag. Table 6 gives the energy results for the Ag*(^{2}D)He$_n$ clusters; as in the case of Cu, we provide data for the first, third and fifth electronic states. Comments similar to those given for copper in the ^{2}D manifold can be made for silver, the only difference is a slightly weaker binding and, consequently, lower $\Delta_0^{\lambda}(n)$ for Ag than for Cu. Given the heavier mass for Ag, which should lower the ground state energy for identical potentials, this finding must be due to slightly shallower potential wells for Ag than for Cu (see Table 1).

The simulation results obtained in this work become useful when it comes to support or help interpreting the experimental results on the fluorescence of Ag atoms in cold He gas obtained exciting the D2 line (*i.e.* the $^2P_{3/2} \leftarrow {}^2$S transition).[19] From these experiments, it emerged that, first, the lifetime ($t_{1/2} \sim 350$ ns) of the D1 and AgHe$_{1,2}$ $^2P_{3/2} \rightarrow {}^2$S fluorescence lines measured when the temperature of the He gas is above the critical temperature T_c is very long compared to the related D2 line of the free silver, and, second, that $t_{1/2}$ drops to roughly 20 ns over a narrow temperature range when $T < T_c$.

The mechanism suggested to explain the long lifetime for those transitions, their sudden drop and the presence of the D1 line in the first place prescribes that Ag in the $^2P_{3/2}$ state captures one or two He atoms forming AgHe$_{1,2}$ in the $^2\Pi_{3/2}$ state. The latter crosses the curve of the $^2\Pi_{5/2}$ state formed when Ag is in the $^2D_{5/2}$ state, which is metastable. Given the relative position of the minima for the two $^2\Pi$ states, the crossing leads to the ejection of the He atoms and the production of the long living ^{2}D state of Ag, the transition to the ^{2}S ground state being doubly forbidden but still weakly visible in the spectrum. It is this state that, acting as a reservoir, can rebuild the population of AgHe$_{1,2}$ or being depopulated collisionally into the $^2P_{1/2}$ state. When $T < T_c$, however, it is in principle possible that He atoms would ''condense'' onto the

Table 7 DMC binding energy $E_0^{\lambda}(n)$ and negative evaporation energy $\Delta_0^{\lambda}(n)$ for the first, third and fifth states (λ = 1,3,5) of Au*(^{2}D)He$_n$

n	$E_0^1(n)^a$	$\Delta_0^1(n)^a$	$E_0^3(n)^a$	$\Delta_0^3(n)^a$	$E_0^5(n)^a$	$\Delta_0^5(n)^a$
1	3.80		3.55		4.02	
2	7.95	−4.15	7.42	−3.87	8.00	−3.98
3	12.04	−4.09	11.45	−4.03	12.18	−4.18
4	16.39	−4.35	15.66	−4.21	16.45	−4.26
5	20.71	−4.32	19.90	−4.23	20.81	−4.36
6	25.22	−4.53	24.5	−4.59	25.2	−4.42
8	34.3	−4.5	33.1	−4.3	33.9	−4.4

[a] Energies in cm^{-1}. The standard error of mean values is roughly one unit of the last decimal digit shown.

^{2}D Ag, thus forming any of the exciplexes indicated as stable in Table 6. These were previously only postulated in ref. 19.

In this respect, it seems worth noticing that the He evaporation energy for those species is roughly 10–11 K per atom, *i.e.* a factor of two larger than T_c; it thus seems sensible to assume the formation of a He ''jacket'' surrounding the silver atom. Such a ''jacket'' presents the helium atoms concentrated in the range of distances 3–9 Å (see Fig. 4, bottom). In the same range, the AgHe $^2\Pi_{1/2}$ potential has its entrance barrier, with a maximum height of 102.1 cm^{-1} with respect to the asymptotic fragments around 3.5 Å (see Fig. 2). This means that the $^2P_{1/2}$ electronic state may have an energy 102–1020 cm^{-1} (depending on the number n of helium atoms) higher than the isolated silver if surrounded by He atoms in a geometry compatible with the one of the stable $^2D_{5/2}$ exciplexes, indicating as possible the crossing between the states and the consequent depopulation by non-adiabatic non-radiative transition. Bearing in mind the 43 cm^{-1} stabilisation due to the He binding to the metal in the ^{2}D state, n = 6–7 should suffice, in principle, to bridge the 690 cm^{-1} gap between the $^2P_{1/2}$ and $^2D_{5/2}$ states. It would of course be interesting to dynamically simulate the process, a task that requires to solve the equations of motion for the mixed Ag–He gas system and that we therefore consider outside the goal of this work for the moment.

4.2.3 Au. Table 7 provides the results for the exciplexes Au*(^{2}D)He$_n$ that we found stable with our simulation procedure. Owing to the weaker Au–He interaction than in the Ag and Cu cases, the binding energy for the gold exciplexes is lower than for the other two metals. For the same reason, the maximum number of first shell He atoms seems to be lower. Similar to the other two metals, the He density surrounding the Au atom is close to spherical. As also the relative position on the energetic scale of the ^{2}P and ^{2}D manifolds of gold parallels what found for copper, it becomes thus possible to justify the lack of the Au D2 fluorescence line found in solid He[8] with arguments similar to the one exposed for Cu.

5 Conclusions

In this work, we have studied the structural and energetic details of exciplexes formed by a coinage metal atom in its lowest ^{2}P and ^{2}D manifolds and a few He atoms. This task was carried out by simulating the exciplex vibrational ground state with DMC, which is capable of exactly sampling the ground state wave function Ψ_0 of strongly anharmonic and fluxional systems. As for the interaction potentials, we employed the DIM approach to build many-body surfaces including spin–orbit coupling starting from atomic spectroscopic data and diatomic interaction surfaces. The latter have been obtained previously for the ^{2}P state of Cu and Ag[34] and in this work for their ^{2}D states, as well as for the ^{2}P and ^{2}D manifolds of Au employing ''state of the art'' CI calculations with extended basis sets. The inclusion of the spin–orbit coupling has required developing the spin–orbit matrix for the d^9s^2 configurations as well as the representation of the dimer Σ, Π and Δ interactions for a general orientation of M*(^{2}D)–He(^{1}S) in the laboratory frame. We hope these would be of help to the community interested in modelling the anisotropic nature of atom–atom interactions.

With respect to the number of He atoms, we focused on studying the details of the inner solvation shell of each excited state, which is relevant for interpreting the emission spectra of Cu, Ag and Au in bulk He and cold He gas. In fact, our results provide full support, albeit only from the energetics point of view, to several of the explanations proposed to justify line disappearance or non-radiative population of the state lying in between the ground and directly excited states. However, the complete description of the mechanisms involved in these experimental phenomena would, in principle, require also the simulation of the post-excitation dynamics with a particular focus on its non-adiabatic components.[70] As helium is intrinsically quantum in nature, this would require at least a semi-classical approach such as zero-point averaged dynamics.[71,72] With the potential energy curves for the excited metal at our disposal, we plan to tackle the study of the dynamical evolution in the near future. Noteworthily, we would expect the case of Ag to be an interesting one, as it would require to correctly describe the mixing between the ^{2}P and ^{2}D manifolds for a proper description. This extra requirement is due to the fact that the $^2D_{5/2}$ state lies in between $^2P_{1/2}$ and $^2P_{3/2}$.

Acknowledgements

MM acknowledges useful discussion with Gabriele Morosi and Dario Bressanini, as well as some assistance with symbolic algebra packages used in developing the interaction matrix **M**. FC acknowledges funding from the Ministero dell'Università e della Ricerca (Project PRIN ''THEORETICAL AND COMPUTATIONAL SIMULATIONS OF QUANTUM MOLECULAR PROCESSES'').

References

1 J. L. Persson, Q. Hui, Z. J. Jakubek, M. Nakamura and M. Takami, *Phys. Rev. Lett.*, 1996, **76**, 1501–1504.
2 Y. Moriwaki and N. Morita, *Eur. Phys. J. D*, 1999, **5**, 53–57.
3 D. Nettels, A. Hofer, P. Moroshkin, R. Müller-Siebert, S. Ulzega and A. Weis, *Phys. Rev. Lett.*, 2005, **94**, 063001.
4 P. Moroshkin, A. Hofer, D. Nettels, S. Ulzega and A. Weis, *J. Chem. Phys.*, 2006, **124**, 024511.

5 Y. Moriwaki, K. Inui, K. Kobayashi, F. Matsushima and N. Morita, *J. Mol. Struct.*, 2006, **786**, 112–117.
6 A. Hofer, P. Moroshkin, D. Nettels, S. Ulzega and A. Weis, *Phys. Rev. A: At., Mol., Opt. Phys.*, 2006, **74**, 032509.
7 P. Moroshkin, A. Hofer, V. Lebedev and A. Weis, *Phys. Rev. A: At., Mol., Opt. Phys.*, 2008, **78**, 032501.
8 P. Moroshkin, V. Lebedev and A. Weis, *J. Low Temp. Phys.*, 2011, **162**, 710–717.
9 P. Moroshkin, V. Lebedev and A. Weis, *Phys. Rev. A: At., Mol., Opt. Phys.*, 2011, **84**, 052519.
10 J. Reho, J. Higgins, C. Callegari, K. K. Lehmann and G. Scoles, *J. Chem. Phys.*, 2000, **113**, 9686–9693.
11 J. Reho, J. Higgins, K. K. Lehmann and G. Scoles, *J. Chem. Phys.*, 2000, **113**, 9694–9701.
12 J. Reho, U. Merker, M. R. Radcliff, K. K. Lehmann and G. Scoles, *J. Chem. Phys.*, 2000, **112**, 8409–8416.
13 J. H. Reho, U. Merker, M. R. Radcliff, K. K. Lehmann and G. Scoles, *J. Phys. Chem. A*, 2000, **104**, 3620–3626.
14 O. Bünermann, M. Mudrich, M. Weidemüller and F. Stienkemeier, *J. Chem. Phys.*, 2004, **121**, 8880–8886.
15 C. P. Schulz, P. Claas and F. Stienkemeier, *Phys. Rev. Lett.*, 2001, **87**, 153401.
16 F. R. Brühl, R. A. Trasca and W. E. Ernst, *J. Chem. Phys.*, 2001, **115**, 10220–10224.
17 M. Mudrich, F. Stienkemeier, G. Droppelmann, P. Claas and C. P. Schulz, *Phys. Rev. Lett.*, 2008, **100**, 023401.
18 G. Auböck, J. Nagl, C. Callegari and W. E. Ernst, *Phys. Rev. Lett.*, 2008, **101**, 035301.
19 Z. J. Jakubek, Q. Hui and M. Takami, *Phys. Rev. Lett.*, 1997, **79**, 629–632.
20 K. Hirano, K. Enomoto, M. Kumakura, Y. Takahashi and T. Yabuzaki, *Phys. Rev. A: At., Mol., Opt. Phys.*, 2003, **68**, 012722.
21 K. Enomoto, K. Hirano, M. Kumakura, Y. Takahashi and T. Yabuzaki, *Phys. Rev. A: At., Mol., Opt. Phys.*, 2004, **69**, 012501.
22 Y. Fukuyama, Y. Moriwaki and Y. Matsuo, *Phys. Rev. A: At., Mol., Opt. Phys.*, 2007, **75**, 032725.
23 Y. Fukuyama, Y. Moriwaki and Y. Matsuo, *Phys. Rev. A: At., Mol., Opt. Phys.*, 2004, **69**, 042505.
24 F. Stienkemeier and A. F. Vilesov, *J. Chem. Phys.*, 2001, **115**, 10119–10137.
25 H. Partridge, J. R. Stallcop and E. Levin, *J. Chem. Phys.*, 2001, **115**, 6471–6488.
26 J. Pascale, *Phys. Rev. A: At., Mol., Opt. Phys.*, 1983, **28**, 632–644.
27 Z. Jakubek and M. Takami, *Chem. Phys. Lett.*, 1997, **265**, 653–659.
28 M. Leino, A. Viel and R. E. Zillich, *J. Chem. Phys.*, 2008, **129**, 184308.
29 M. Leino, A. Viel and R. E. Zillich, *J. Chem. Phys.*, 2011, **134**, 024316.
30 D. Dell'Angelo, G. Guillon and A. Viel, *J. Chem. Phys.*, 2012, **136**, 114308.
31 M.-C. Heitz, L. Teixidor, N.-T. Van-Oanh and F. Spiegelman, *J. Phys. Chem. A*, 2010, **114**, 3287–3296.
32 T. Takayanagi and M. Shiga, *Phys. Chem. Chem. Phys.*, 2004, **6**, 3241–3247.
33 A. Wada, T. Takayanagi and M. Shiga, *J. Chem. Phys.*, 2003, **119**, 5478–5486.
34 F. Cargnoni and M. Mella, *J. Phys. Chem. A*, 2011, **115**, 7141–7152.
35 F. O. Ellison, *J. Am. Chem. Soc.*, 1963, **85**, 3540–3544.
36 F. Federmann, K. Hoffmann, N. Quaas and J. D. Close, *Phys. Rev. Lett.*, 1999, **83**, 2548–2551.
37 M. Patrone and M. Mella, *Chem. Phys. Lett.*, 2011, **514**, 16–20.
38 D. Figgen, G. Rauhut, M. Dolg and H. Stoll, *Chem. Phys.*, 2005, **311**, 227–244.
39 M. Mella, M. Colombo and G. Morosi, *J. Chem. Phys.*, 2002, **117**, 9695–9702.
40 M. W. Schmidt, K. K. Baldridge, J. A. Boatz, S. T. Elbert, M. S. Gordon, J. H. Jensen, S. Koseki, N. Matsunaga, K. A. Nguyen, S. J. Su, T. L. Windus, M. Dupuis and J. A. Montgomery, *J. Comput. Chem.*, 1993, **14**, 1347–1363.
41 H.-J. Werner, P. J. Knowles, G. Knizia, F. R. Manby and M. Schütz, *Wiley Interdiscip. Rev.: Comput. Mol. Sci.*, 2012, **2**, 242–253.
42 H.-J. Werner, P. J. Knowles, G. Knizia, F. R. Manby, M. Schütz, T. K. P. Celani, R. Lindh, A. Mitrushenkov, G. Rauhut, K. R. Shamasundar, T. B. Adler, R. D. Amos, A. Bernhardsson, A. Berning, D. L. Cooper, M. J. O. Deegan, A. J. Dobbyn, F. Eckert, E. Goll, C. Hampel, A. Hesselmann, G. Hetzer, T. Hrenar, G. Jansen, C. Köppl, Y. Liu, A. W. Lloyd, R. A. Mata, A. J. May, S. J. McNicholas, W. Meyer, M. E. Mura, A. Nicklass, D. P. O'Neill, P. Palmieri, D. Peng, K. Pflüger, R. Pitzer, M. Reiher, T. Shiozaki, H. Stoll, A. J. Stone, R. Tarroni, T. Thorsteinsson and M. Wang, http://www.molpro.net, 2012.
43 C. H. P. J. Knowles and H.-J. Werner, *J. Chem. Phys.*, 1993, **99**, 5219–5227.
44 S. Boys and F. Bernardi, *Mol. Phys.*, 1970, **19**, 553–566.
45 K. A. Peterson and C. Puzzarini, *Theor. Chem. Acc.*, 2005, **114**, 283–296.
46 D. E. Woon and T. H. Dunning Jr., *J. Chem. Phys.*, 1994, **100**, 2975–2988.
47 F.-M. Tao, Z. Li and Y.-K. Pan, *Chem. Phys. Lett.*, 1996, **255**, 179–186.
48 J. Klos, M. Rode, J. Rode, G. Chalasinski and M. Szczesniak, *Eur. Phys. J. D*, 2004, **31**, 429–437.
49 J. E. Huheey, *Inorganic Chemistry: Principles of Structure and Reactivity*, Harper International, New York, USA, 3rd edn, 1993.
50 N. Brahms, T. V. Tscherbul, P. Zhang, J. Klos, R. C. Forrey, Y. S. Au, H. R. Sadeghpour, A. Dalgarno, J. M. Doyle and T. G. Walker, *Phys. Chem. Chem. Phys.*, 2011, **13**, 19125–19141.
51 H. R. S. J. Loreau and A. Dalgarno, *J. Chem. Phys.*, 2013, **138**, 084301.
52 F. Cargnoni, T. Kuś, M. Mella and R. J. Bartlett, *J. Chem. Phys.*, 2008, **129**, 204307.
53 F. Dalfovo, A. Lastri, L. Pricaupenko, S. Stringari and J. Treiner, *Phys. Rev. B: Condens. Matter Mater. Phys.*, 1995, **52**, 1193–1209.

54 J. B. Anderson, *J. Chem. Phys.*, 1975, **63**, 1499–1503.
55 B. L. Hammond, W. A. Lester and P. J. Reynolds, *Monte Carlo Methods in Ab Initio Quantum Chemistry*, World Scientific, Singapore, 1994.
56 P. Håkansson and M. Mella, *J. Chem. Phys.*, 2007, **126**, 104106.
57 P. Slavicek and M. Lewerenz, *Phys. Chem. Chem. Phys.*, 2010, **12**, 1152–1161.
58 V. Buch, P. Sandler and J. Sadlej, *J. Phys. Chem. B*, 1998, **102**, 8641–8653.
59 M. H. Kalos, *J. Comput. Phys.*, 1966, **1**, 257–276.
60 M. Mella and D. C. Clary, *J. Chem. Phys.*, 2003, **119**, 10048–10062.
61 H. Flyvbjerg and H. G. Petersen, *J. Chem. Phys.*, 1989, **91**, 461–466.
62 C. J. Margulis and D. F. Coker, *J. Chem. Phys.*, 2000, **113**, 6113–6121.
63 J. K. Sakurai, *Modern Quantum Mechanics*, Addison-Wesley, Reading, MA, 1995.
64 M. Edén, *Concepts Magn. Reson., Part A*, 2003, **17**, 117–154.
65 E. Cheng and K. B. Whaley, *J. Chem. Phys.*, 1996, **104**, 3155–3175.
66 P. Moroshkin, A. Hofer and A. Weis, *Phys. Rep.*, 2008, **469**, 1–57.
67 J. Dupont-Roc, *Z. Phys. B: Condens. Matter*, 1995, **98**, 383–386.
68 M. Mella, *J. Chem. Phys.*, 2011, **135**, 114504.
69 A. V. Danilychev and V. A. Apkarian, *J. Chem. Phys.*, 1994, **100**, 5556–5566.
70 J. C. Tully, *J. Chem. Phys.*, 1990, **93**, 1061–1071.
71 P. Slavìček, P. Jungwirth, M. Lewerenz, N. Nahler, M. Farnik and U. Buck, *J. Phys. Chem. A*, 2003, **107**, 7743–7754.
72 D. Bonhommeau, M. Lewerenz and N. Halberstadt, *J. Chem. Phys.*, 2008, **120**, 054308.